Received: 19 November 2021 | Revised: 8 March 2022 | Accepted: 24 April 2022

DOI: 10.1002/aic.17741

AIChE JOURNAL

RESEARCH ARTICLE

Process Systems Engineering

Simultaneous mixed-integer dynamic scheduling of processes and their energy systems

Florian Joseph Baader[1,2] | André Bardow[1,3,4] | Manuel Dahmen[1]

[1]Institute of Energy and Climate Research, Energy Systems Engineering (IEK-10), Forschungszentrum Jülich GmbH, Jülich, Germany

[2]Faculty of Mechanical Engineering, RWTH Aachen University, Aachen, Germany

[3]Energy & Process Systems Engineering, ETH Zürich, Zürich, Switzerland

[4]Institute of Technical Thermodynamics, RWTH Aachen University, Aachen, Germany

Correspondence
Manuel Dahmen, Forschungszentrum Jülich GmbH, Institute of Energy and Climate Research, Energy Systems Engineering (IEK-10), Jülich 52425, Germany.
Email: m.dahmen@fz-juelich.de

Funding information
Helmholtz-Gemeinschaft, Grant/Award Number: Energy System 2050 (ES2050)

Abstract

Increasingly volatile electricity prices make simultaneous scheduling optimization desirable for production processes and their energy systems. Simultaneous scheduling needs to account for both process dynamics and binary on/off-decisions in the energy system leading to challenging mixed-integer dynamic optimization problems. We propose an efficient scheduling formulation consisting of three parts: a linear scale-bridging model for the closed-loop process output dynamics, a data-driven model for the process energy demand, and a mixed-integer linear model for the energy system. Process dynamics is discretized by collocation yielding a mixed-integer linear programming (MILP) formulation. We apply the scheduling method to three case studies: a multiproduct reactor, a single-product reactor, and a single-product distillation column, demonstrating the applicability to multiple input multiple output processes. For the first two case studies, we can compare our approach to nonlinear optimization and capture 82% and 95% of the improvement. The MILP formulation achieves optimization runtimes sufficiently fast for real-time scheduling.

KEYWORDS
demand response, integration of scheduling and control, mixed-integer dynamic optimization, mixed-integer linear programming, simultaneous scheduling

1 | INTRODUCTION

Current efforts to reduce greenhouse gas emissions increase the share of renewable electricity production in many countries. Due to the intermittent nature of renewable electricity production, stronger volatility in electricity prices or even electricity availability is expected.[1] This price volatility may offer economic benefits to industrial processes that can dynamically adapt their operation and thus their power consumption in so-called demand response (DR).[2] Ideally, DR reacts to imbalances of electricity demand and supply and therefore also stabilizes the electricity grid.[3]

A promising way to achieve DR is to consider volatile prices in scheduling optimization[1] that determines the process operation for a time horizon in the order of 1 day.[4–6] However, industrial processes are often not supplied directly by the electricity grid but by a local on-site multienergy system. The local multienergy system supplies all energy demanded by the process, for example, heating, cooling, or electricity, and exchanges electricity with the grid.[7] Operating local energy systems is a complex task as these systems typically consist of multiple redundant units with non-linear efficiency curves and minimum part-load constraints leading to discrete on/off-decisions.[7] Thus, the electricity exchange between the energy system and the grid is not directly proportional to the process energy demand. Consequently, optimal DR scheduling must consider processes and their energy systems simultaneously. Moreover, such simultaneous scheduling can improve the efficiency of energy system operation by

shifting process energy demand in time.[8] Still, scheduling is usually carried out sequentially: the process schedule is optimized first and only then the energy system operation is optimized.[9,10]

The simultaneous scheduling of processes and their energy systems leads to computationally challenging problems. Process scheduling can already be a very demanding task on its own if nonlinear process dynamics need to be considered[11]; therefore, considering dynamics is a major research topic in process systems engineering referred to as integration of scheduling and control.[4,5,12–15] For DR problems, process dynamics is often scheduling-relevant[2,4,5,16,17] because the time to drive the process from one steady state to another steady state is often in the same order of magnitude as the electricity-price time steps.

The desired simultaneous scheduling of processes and their energy systems is especially challenging due to the simultaneous presence of process dynamics and discrete on/off-decisions in the energy system (Figure 1). Because of the discrete decisions, standalone energy system optimization problems are preferably formulated as mixed-inter linear programs (MILPs).[7,18–21] A MILP formulation is usually applicable because: (a) nonlinear part-load efficiencies can be approximated reasonably well using piece-wise affine functions,[21] and (b) the dynamics of the energy system units is negligible or can be captured using ramping constraints.[22]

As process dynamics is often scheduling-relevant, the simultaneous scheduling needs to be integrated with control. Even though conceptually, all approaches for the integration of scheduling and control can be used, the on/off-decisions significantly increase the computational complexity. However, scheduling must be performed online. Harjunkoski et al.[23] state that generally optimization run times should be between 5 and 20 min.

In this work, we present a formulation for simultaneous scheduling of processes and their energy systems that aims at real-time-applicable runtimes. We rely on two promising approaches from the integration of process scheduling and control: (i) dynamic scale-bridging models (SBMs),[24,25] where the controlled process output is forced to follow a linear differential equation and (ii) dynamic data-driven models.[2,26–28] Specifically, our formulation consists of three parts: (i) a SBM considering the dynamics of the production process, (ii) a piece-wise affine dynamic data-driven model for the energy demand of the process, and (iii) a MILP energy system model with piece-wise affine approximations of nonlinear component efficiency curves. We discretize the linear differential equations in time using a high-order collocation scheme to receive linear constraints.[29] Consequently, we achieve an MILP formulation for the entire scheduling problem.

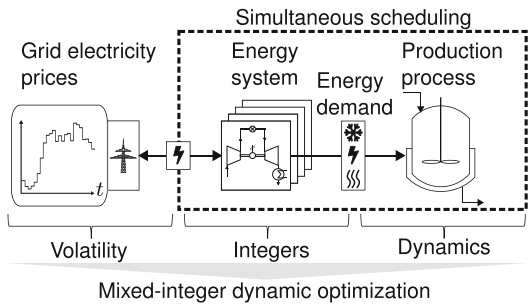

FIGURE 1 Volatile grid electricity prices call for a simultaneous scheduling of production processes and their local energy supply systems. While energy systems introduce integer decision variables, processes often exhibit scheduling-relevant dynamics. Simultaneous scheduling thus results in computationally challenging mixed-integer dynamic optimization (MIDO) problems.

A preliminary version of our approach has been presented in a conference contribution[30] where we considered DR for a building energy system. In the present contribution, we describe our method in more detail and apply it to three chemical production systems: a multi-product and a single-product continuous stirred tank reactor (CSTR) both of which are cooled by three compression chillers (CCs), and a distillation column heated by two combined heat and power plants (CHPs) and an electricity-driven boiler (EB). The new method is explicitly compared against a standard sequential scheduling approach from industrial practice.[9] The remainder of this article is structured as follows: in Section 2, the method is described in detail. In Section 3, a first case study considering a multiproduct CSTR is performed; in Section 4, a second case study considering a single-product CSTR is performed; and in Section 5, a third case study considering a distillation column is investigated. Section 6 concludes the work.

2 | METHOD

In this section, we present our method for simultaneous dynamic scheduling (SDS) of production processes and their energy systems. We refer to our method as SDS. The core of SDS is an efficient scheduling model consisting of three parts: (i) the production process, (ii) the energy demand, and (iii) the energy system (Figure 2). Model (i) determines the controlled process output y_{cv}, for example, the concentration in a reactor. We use a SBM proposed by Baldea and coworkers[24,25] that describes a linear closed-loop response and represents the slow scheduling-relevant dynamics only. A linear SBM can be incorporated in scheduling optimization much more efficiently than a nonlinear full-order process model. The SBM relies on an underlying control to enforce the desired linear closed-loop response. The closed-loop response describes the evolution of the controlled variable y_{cv} and its time derivatives depending on the set-point w_{SP}:

$$y_{cv} + \sum_{i=1}^{r} \tau_i \frac{d^i y_{cv}}{dt^i} = w_{SP}. \quad (1)$$

In Equation (1), r is the order of the SBM and τ_i is the time constant. We discuss both order and time constants in the following subsection. To linearize the closed-loop response, we propose to place a set-point filter[31] in front of the controlled plant (Figure 2). This set-point filter converts the piece-wise constant set-point w_{SP} given by the scheduling optimization to a smooth filtered set-point $w_{SP,fil}$ that can be

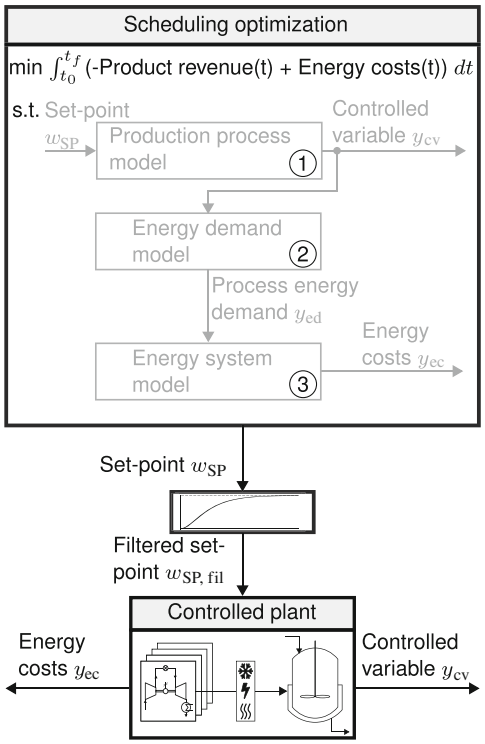

FIGURE 2 Proposed simultaneous scheduling of processes and their energy systems based on our scheduling model consisting of three parts. A set-point filter converts the optimized piece-wise constant set-point w_{SP} to a smooth filtered set-point $w_{SP,fil}$, which defines the desired linear closed-loop process behavior.

tracked by the underlying process control such that $y_{cv} \approx w_{SP,fil}$. In essence, we assume that the linear dynamics of the set-point filter can model the process output dynamics for the scheduling-relevant time scale. Instead of the combination of set-point filter and tracking control, previous publications used exact input–output feedback linearization[24,31,32] or scheduling-oriented model predictive control (SO-MPC).[25] The proposed set-point filter increases the flexibility of the scale-bridging approach as it allows to use non-model-based tracking controls, for example, PID-control,[31] as well.

A disadvantage of the SBM is the resulting conservatism because the time constants need to be chosen such that the desired linear closed-loop response can be realized in all operating regimes. Therefore, the closed-loop response is slower than necessary in some operating regimes.

The main advantage is that the scale-bridging Equation (1) is more than an approximation: whenever the actual value of y_{cv} deviates from the closed-loop response described by Equation (1), the underlying control acts to bring the controlled variable y_{cv} back to the desired closed-loop trajectory. Consequently, deviations of the controlled variable from its optimized trajectories are kept small.

Note that, in this article, we study the case of a single SBM, whose application is straightforward for single-input single-output (SISO) processes where the SBM deals with the only controlled variable y_{cv}. In the multiple input multiple output (MIMO) case, a vector of output variables $\mathbf{y}_{cv}$ is controlled; still, the number of slow scheduling-relevant variables is typically small.[4,25,26] Moreover, for flexible DR operation, often, only one scheduling-relevant quantity ρ is varied to shift energy demand in time, for example, the production rate or product purity. A single SBM for this quantity ρ is sufficient if all controlled outputs are either maintained constant irrespective of the scheduling-relevant quantity ρ or are alternatively coupled with ρ. For instance, the hold-up of process units might be maintained constant irrespective of flexible operation. An example for coupling of controlled process outputs is given in the initial SBM paper where Du et al.[24] consider a reactor with concentration and temperature as controlled outputs but only an SBM of the concentration during scheduling. After scheduling, Du et al. derive a set-point signal for the temperature from the set-point signal of the concentration. Consequently, often, only one SBM needs to be tuned even though multiple inputs and outputs are present. Such a case is also shown in our third case study, where we consider a 4×4 MIMO process.

Model (ii) is a dynamic data-driven model[2] that determines the process energy demand y_{ed} taking the current state of the production process as inputs, that is, the controlled variable y_{cv} and its time derivatives. In principle, a wide range of dynamic data-driven models derived from recorded data, or mechanistic models can be used here. Examples of dynamic data-driven models being applied successfully in dynamic DR optimization can be found in the literature.[26–28,33] Our energy demand model (ii) can be dynamic and mixed-integer but must be linear as we aim for an MILP formulation. Note that the energy demand can, in general, not only depend on the controlled outputs but also on other uncontrolled states. In such cases, the data-driven energy demand model needs to have internal states that approximate the internal dynamics of the real process. Models with internal states, such as Hammerstein-Wiener models, are common in system identification and have also been used in demand-response applications.[28] An energy demand model with an internal state is demonstrated in our third case study.

In contrast to the controlled process output y_{cv}, deviations between the actual process energy demand y_{ed} and the model prediction are not corrected. Instead, we assume that such deviations are compensated by the energy system, which is reasonable if (a) the energy system can react significantly faster than the process and (b) the energy system has spare capacity larger than the maximum error of the data-driven model.

In this article, we assume that the energy demand is the only uncontrolled process quantity that is relevant for the scheduling objective function. In principle, other uncontrolled quantities could be relevant for the scheduling objective function as well. For instance, raw material consumption could vary due to flexible operation and thus cause additional costs that should not be neglected in the optimization. In such cases, data-driven models for those quantities need to be derived and added in the same way as for the energy demand.

Model (iii) is the energy system model that determines the energy costs depending on the energy demand. The structure of the energy system is modeled by energy balances that connect the energy system components with demands. Moreover, the efficiency of individual energy system components is modeled as a function of the part-load

fraction. Thus, the required input power $P_{c,\text{in}}$ of an energy system component c is a nonlinear function of the desired output power $P_{c,\text{out}}$.[21] To obtain an MILP formulation, we follow the established approach of modeling part-load efficiency curves as piece-wise affine functions.[7] In general, piece-wise affine efficiency curves require binary variables. Binary variables increase the computational burden; however, they can be avoided if the input power is a convex function of the output power,[20] which is the case for many energy system components of practical relevance.[7]

By combining the three models (i)–(iii), we receive a linear differential algebraic equation system (DAE) containing integers:

$$\frac{d\mathbf{x}}{dt} = \mathbf{f}(\mathbf{x},\mathbf{y},\mathbf{z},\mathbf{w}_{\text{SP}}) = \mathbf{A}\mathbf{x} + \mathbf{B}\mathbf{y} + \mathbf{C}\mathbf{z} + \mathbf{D}\mathbf{w}_{\text{SP}}, \tag{2}$$

$$\mathbf{0} = \mathbf{g}(\mathbf{x},\mathbf{y},\mathbf{z},\mathbf{w}_{\text{SP}}) = \mathbf{E}\mathbf{x} + \mathbf{F}\mathbf{y} + \mathbf{G}\mathbf{z} + \mathbf{H}\mathbf{w}_{\text{SP}}. \tag{3}$$

In Equations (2) and (3), $\mathbf{x}$ is the differential state, $\mathbf{y}$ is the continuous variable, $\mathbf{z}$ is the discrete variable, $\mathbf{w}_{\text{SP}}$ is the set-point, t is time, $\mathbf{f}$ and $\mathbf{g}$ are functions that are linear in $\mathbf{x}$, $\mathbf{y}$, $\mathbf{z}$, $\mathbf{w}_{\text{SP}}$, and $\mathbf{A}$–$\mathbf{H}$ are matrices. Note that all variables are functions of time although not stated explicitly to improve readability.

We choose a discrete-time MILP formulation for our simultaneous scheduling problem because in case of variable electricity prices, discrete-time formulations usually perform better than continuous-time formulations,[34] as the electricity markets imposes a discrete time structure, for example, hourly constant prices. As our model consists of linear differential equations, time discretization with collocation in discrete time leads to linear constraints.[29]

In the following, we discuss the SBM parameters and the scheduling optimization problem.

2.1 | Scale-bridging model parameters

For the SBM (i), we have to determine the order r and the time constants τ_i from Equation (1), as well as upper and lower bounds for the set-point $w_{\text{SP}}^{\max}$, $w_{\text{SP}}^{\min}$, respectively. The order r should be chosen such that the resulting reference trajectory for the controlled variable y_{cv} can be realized by the process. For instance, if a process reacts with second-order dynamics to input changes, a first-order set-point filter is not reasonable. Thus, the order r should reflect how many stages of inertia a change in the manipulated variable u has to overcome before changing the controlled variable y_{cv}. If a process model is available, the order r can be derived mathematically by analyzing the relative degree of the process model defined as the number of times the controlled variable y_{cv} has to be differentiated with respect to time until the manipulated variable u appears explicitly.[31] If no process model is available, the order r needs to be chosen based on knowledge or intuition about the main inertia of the process. In this way, the set-point filter reflects the characteristics of the open-loop system. The employed controller might add additional dynamics to the closed-loop system, for instance, the integral part of a PI-controller. Using the relative order of the open-loop process to choose the relative order of the set-point filter is thus only reasonable if it can be assumed that either the controller dynamics are significantly faster than the process dynamics or the proportional part of the controller dominates over the integral part. That is, our approach might not work well in a case where the controller adds significant dynamics to the closed-loop system. In such a case, the controller can be changed, or alternative approaches that explicitly model the control behavior might be used instead. For instance, Dias et al.[35] optimize a schedule using a sequential optimization approach with the controller being part of the simulation model. Thus, they optimize the closed-loop system. Remigio and Swartz[36] explicitly account for the behavior of an underlying model predictive controller (MPC) by adding the KKT-conditions of the MPC to the scheduling optimization problem.

As discussed by Baldea et al.,[25] the choice of the time constants τ_i is critical for the performance of the scale-bridging approach: on the one hand, if the time constants are too small, the scale-bridging dynamics is too fast and cannot be realized by the controlled process. On the other hand, if the time constants are too large, the scale-bridging dynamics is overly conservative and process flexibility is wasted. However, a rigorous way to tune the time constants τ_i is missing in the literature.

In this article, we argue that the time constants τ_i need to be tuned simultaneously with the set-point bounds $w_{\text{SP}}^{\max}$ and $w_{\text{SP}}^{\min}$. For illustration, we consider a transition of the controlled variable starting from a small value $y_{\text{cv}}^{\text{start}}$ and ending at a new steady state with a higher value $y_{\text{cv}}^{\text{end}}$ close to the maximum allowable value $y_{\text{cv}}^{\max}$. To speed up the transition, scheduling optimization might choose a set-point $w_{\text{SP,elevated}}$ which is elevated above $y_{\text{cv}}^{\text{end}}$ and even $y_{\text{cv}}^{\max}$ for a certain period of time. However, choosing an elevated set-point value can lead to dynamics that are too fast for the controlled process. In particular, if the time constants τ_i are small, the scale-bridging dynamics is already fast and an elevated set-point may drive the controlled variable to infeasible values. A trade-off arises because we want to choose small time constants in general but also want to avoid slow transitions toward the bounds of the controlled variable.

In our case studies, we tune the scale-bridging parameters using a simple heuristic relying on simulations. Alternatively, existing knowledge about the time constants of the process, or measurements can be used to calibrate the SBM.

2.2 | Scheduling optimization problem

To derive a complete problem formulation based on Equations (2) and (3), we add a suitable objective function, discretize time, and add inequality constraints to account for variable bounds, minimum part-load, and problem-specific constraints.

The objective Φ in simultaneous DR scheduling is to maximize cumulative product revenue Φ_{Product} at final time t_f minus the cumulative energy costs Φ_{Energy} at final time:

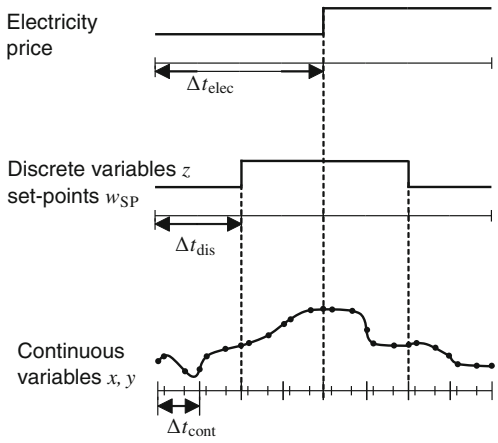

FIGURE 3 Three time grids used for discretization with timesteps Δt_{elec}, Δt_{dis}, Δt_{cont}, respectively

$$\min \Phi = -\Phi_{\text{Product}}(t_f) + \Phi_{\text{Energy}}(t_f), \tag{4}$$

$$\frac{d\Phi_{\text{Product}}}{dt} = \sum_{p \in \mathbb{P}} K_p q_p, \tag{5}$$

$$\frac{d\Phi_{\text{Energy}}}{dt} = \sum_{e \in \mathbb{E}} K_e P_e \quad \text{with } \Phi_{\text{Product}}(t_0) = \Phi_{\text{Energy}}(t_0) = 0. \tag{6}$$

Here, $\mathbb{P}$ is the set of products, q_p the flow rate of product p, and K_p the price of p. Similarly, $\mathbb{E}$ is the set of end-energy forms consumed, K_e is the time-dependent price of energy e, and P_e is the consumed power of energy e. t_0 denotes the initial time.

For time discretization, we use three time grids (Figure 3). Grid 1 is given by the electricity market and contains piece-wise constant electricity prices with time step Δt_{elec}, for example, 1 h or 15 min. Grid 2 contains discrete decision variables $\mathbf{z}$ and piece-wise constant set-points $\mathbf{w}_{SP}$. The resolution of grid 2 should not be too fine as it increases the number of integer variables and thus the combinatorial complexity of the optimization problem. Still, it should be possible to alter discrete decisions $\mathbf{z}$ and set-points $\mathbf{w}_{SP}$ at least at every step change of electricity prices. Thus, the electricity price time step resolution should constitute a lower bound on the resolution of grid 2. Making grid 2 finer than grid 1 by selecting time steps $\Delta t_{dis} < \Delta t_{elec}$, gives a higher flexibility and thus might enable higher profits. We recommend to use time steps with lengths $\Delta t_{dis} = \frac{1}{n_1}\Delta t_{elec}$ with n_1 being a small natural number.

Grid 3 is used for continuous variables $\mathbf{x}$, $\mathbf{y}$. Differential states $\mathbf{x}$ are discretized using collocation. Similar to the argument above, we propose to use finite elements with length $\Delta t_{cont} = \frac{1}{n_2}\Delta t_{dis}$. The natural number n_2 is chosen to be greater than or equal to one because whenever electricity prices, discrete variables, or set-points perform step-changes, a new collocation element is necessary such that non-smoothness in differential states $\mathbf{x}$ is possible. In result, **states** $\mathbf{x}$ are continuous at the border of collocation elements but first derivatives are allowed to perform step changes.

Within a finite element f_e of grid 3, a collocation polynomial x_{f_e} of order N_{cp} is used to discretize differential states[29,37]:

$$x_{f_e}(\bar{\tau}) = \sum_{j=0}^{N_{cp}} l_j(\bar{\tau}) x_{f_e j}, \quad \bar{\tau} \in [0,1], \tag{7}$$

$$l_j = \prod_{k=0, k \neq j}^{N_{cp}} \frac{\bar{\tau} - \bar{\tau}_k}{\bar{\tau}_j - \bar{\tau}_k}, \tag{8}$$

$$\left.\frac{dx}{dt}\right|_{t_{f_e k}} = \frac{1}{\Delta t_{cont}} \sum_{j=0}^{N_{cp}} x_{f_e j} \frac{dl_j(\bar{\tau}_k)}{d\bar{\tau}}. \tag{9}$$

In Equations (7) and (8), the l_j are Lagrange basis polynomial, $\bar{\tau}$ is the scaled time within a finite element, and $x_{f_e j}$ is state value at discretization points. In Equation (9), $\left.\frac{dx}{dt}\right|_{t_{f_e k}}$ is the approximated time derivative at a collocation point k, which is set equal to the right-hand side of the linear differential equation (2) for every time point $t_{f_e,k}$. The term $\frac{dl_j(\bar{\tau}_k)}{d\bar{\tau}}$ is a constant parameter in the optimization because it only depends on $\bar{\tau}$. Moreover, as we choose discrete time, Δt_{cont} is constant. Therefore, $x_{f_e j}$ is the only optimization variable, and thus, discretization with Equation (9) leads to linear constraints.

As inequality constraints, we consider upper and lower bounds for all variables, minimum part-load constraints for energy system components, and problem-specific constraints, for example, minimum production targets. Minimum part-load constraints are realized with a binary variable $z_{on,c}$ that indicates if the output power $P_{c,out}$ of an energy system component c is zero or between the minimal and maximal allowed value, $P_{c,out}^{min}$ and $P_{c,out}^{max}$, respectively:

$$z_{c,on} P_{c,out}^{min} \leq P_{c,out} \leq z_{c,on} P_{c,out}^{max}. \tag{10}$$

Assembling the discussed equations gives the simultaneous scheduling optimization problem for the production process and its energy system.

Our discussion focuses on energy-intensive processes that can be operated flexibly and exhibit scheduling-relevant dynamics. The energy demand of other processes also present at the same chemical production site can be integrated in our MILP scheduling optimization problem in straightforward manner: the energy demand of processes with no or negligible flexibility can be expressed as predefined time-varying demands that can be added to the energy balances as constant terms. For processes with negligible dynamics, quasi-steady state can be assumed and the steady-state energy demand can be modeled as a piece-wise affine function.[38]

3 | CASE STUDY 1: MULTIPRODUCT REACTOR

In this section, we assess the computational performance of our method in a first case study considering a multiproduct reactor. We benchmark the economic value of SDS to a standard sequential scheduling and to a nonlinear scheduling optimization with the true process model.

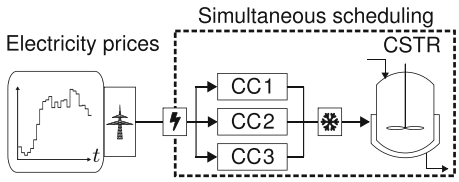

FIGURE 4 Case study 1: simultaneous scheduling of a continuous stirred tank reactor (CSTR) cooled by three compression chillers (CC1, CC2, CC3). Time-varying electricity prices provide an economic incentive for DR.

TABLE 1 Product band $\left[C^{\min}_{A,p}, C^{\max}_{A,p}\right]$ in mol/L, price K^P_p in money unit (MU)/m^3, and cooling power in steady-state production $Q^{\text{steady}}_{\text{cool},p}$ in MJ/h, for products $p \in \{I, II, III\}$

p	$\left[C^{\min}_{A,p}, C^{\max}_{A,p}\right]$	K^P_p	$Q^{\text{steady}}_{\text{cool},p}$
I	[0.09, 0.11]	1	6.05
II	[0.29, 0.31]	0.75	5.43
III	[0.49, 0.51]	0.5	4.65

3.1 | Setup

The setup of the case study is visualized in Figure 4. An exothermic multiproduct CSTR is cooled with three CCs. We use an exemplary reactor model from Petersen et al.[39] In the CSTR, a component *A* reacts to a component *B*. The reactor can produce three products *I*, *II*, *III*, which are defined by the desired concentration of component *A*, C_A. We assume a small tolerance of ±0.01 mol/L such that for each product, we obtain a product band. Whenever the concentration C_A is within one of the three product bands, the associated product is produced. If the concentration is outside of the three product bands, which happens necessarily during transitions, no product is produced. For illustration, we consider prices of 1, 0.75, and 0.5 money unit (MU) (Table 1) and require a minimum daily production of 5 h and a maximum daily production of 8 h for each product.

In the CSTR model, the rate of change for the concentration of component *A* is given by the material balance and the rate of change for the temperature *T* is given by the energy balance:

$$\frac{dC_A}{dt} = \frac{q}{V}(C_{A,\text{feed}} - C_A) - k e^{-\frac{E_A}{RT}} C_A, \tag{11}$$

$$\frac{dT}{dt} = \frac{q}{V}(T_{\text{feed}} - T) - \frac{k\Delta H_r}{\varrho C_P} e^{-\frac{E_A}{RT}} C_A - \frac{Q_{\text{cool}}}{\varrho C_P V}. \tag{12}$$

In Equations (11) and (12), q is the flow rate, V the reactor volume, $C_{A,\text{feed}}$ the feed concentration, k the reaction constant, E_A the activation energy, R the gas constant, T_{feed} the feed temperature, ΔH_r the enthalpy of reaction, ϱ the density, C_P the heat capacity, and Q_{cool} is the cooling provided to the reactor. The parameter values listed in Table S1 are exemplary values from Petersen et al.,[39] except that we varied the activation energy E_A to obtain an operating temperature where cooling with compression chillers is a realistic option.

TABLE 2 Nominal cooling power $Q^{\max}_{CC,i}$ and coefficient of performance $\text{COP}^{\text{nom}}_{CC,i}$ for compression chillers

Compression chiller	$Q^{\max}_{CC,i}$ (MJ/h)	$\text{COP}^{\text{nom}}_{CC,i}$
1	4.8	6
2	2.3	4.5
3	1.5	3

An efficient chiller is used for base-load cooling, whereas chiller 2 has a medium coefficient of performance (COP), and chiller 3, which has a low COP, is used for peak cooling (see Table 2). We use the compression chiller model from Voll et al.[7] with a minimum part load of 20% and a COP depending on nominal COP, $\text{COP}^{\text{nom}}_{CC,i}$, cooling load $Q_{CC,i}$, and nominal cooling load $Q^{\max}_{CC,i}$:

$$\text{COP}_{CC,i} = \text{COP}^{\text{nom}}_{CC,i}\left(0.8615 q^3_{CC,i} - 3.5494 q^2_{CC,i} + 3.679 q_{CC,i} + 0.0126\right), \quad \text{with } q_{CC,i} = \frac{Q_{CC,i}}{Q^{\max}_{CC,i}}. \tag{13}$$

Note that this case study is meant to be an illustrative example rather than a real case. It allows us to study whether the proposed method is able to consider process dynamics and discrete on/off-decisions for energy system components simultaneously. We want to stress that even though the original nonlinear process model is a small-scale model, the resulting SBM (i) would have the same basic structure and computational complexity if a larger process model would be considered as the number of scheduling-relevant dynamics is typically small.[4,25,26]

We employ conventional PID control[31] to track the filtered set-point for the concentration C_A by manipulating the cooling power Q_{cool}:

$$Q_{\text{cool}} = K_P\left(e + \tau_D \frac{de}{dt} + \frac{1}{\tau_I}\int_0^t e dt\right) + Q^{\text{PID},0}_{\text{cool}}, \text{ with } e = w_{\text{SP,fil}} - C_A. \tag{14}$$

The controller parameters in Equation (14) are: K_P, τ_D, τ_I, and $Q^{\text{PID},0}_{\text{cool}}$. We choose $Q^{\text{PID},0}_{\text{cool}}$ to be the steady-state cooling power of product *II* (Table 1) and manually tune the remaining controller parameters in a simulation such that the filtered set-point $w_{\text{SP,fil}}$ is tracked stably and accurately. The resulting parameters are: $K_P = 1000\,\text{MJ L/h mol}$, $\tau_D = 0.1$ h, and $\tau_I = 0.2$ h. The stable and accurate set-point tracking is shown in the following (Figure 6).

3.2 | Simultaneous dynamic scheduling

To apply our SDS method, we now set up the three parts of our model and the scheduling optimization problem as presented in Section 2.

3.2.1 | Scale-bridging production process model

As discussed in Section 2, we need to choose the order r, the time constants τ_i, and the set-point bounds w_{SP}^{min}, w_{SP}^{max} for the scale-bridging production process model (i). The relative order of the open-loop process is 2, as can be seen from the physical process model: the manipulated variable Q_{cool} does not appear in the first derivative of the controlled variable C_A (Equation (11)). If Equation (11) is differentiated with respect to time and the term $\frac{dT}{dt}$ is replaced using Equation (12), the second time derivative $\frac{d^2C_A}{dt^2}$ appears as an explicit function of the input Q_{cool}. Thus, the open-loop system has a relative degree of 2. The more descriptive explanation is that a change in the cooling power Q_{cool} has to first overcome the inertia of the temperature T and then the inertia of the concentration C_A. As discussed in Section 2, we choose the order of the set-point filter equal to the relative order of the open-loop process, that is, $r = 2$. Our simulation results show that the second-order response can in fact be realized by the closed-loop system (Figure 6).

Second-order systems are described in control theory by the time constant of their natural oscillation β and a damping coefficient ζ.[31] The two tunable time constants τ_1 and τ_2 can be expressed as:

$$\tau_1 = 2\zeta\beta, \tag{15}$$

$$\tau_2 = \beta^2. \tag{16}$$

Following Du et al.,[24] we choose a critically damped response, that is, $\zeta = 1$, as we want to have fast but no oscillating dynamics.

In the following, we describe the heuristic procedure used to define the remaining time constant β simultaneously with the bounds for the set-point w_{SP}^{max} and w_{SP}^{min}. The allowed range of the set-point must at least cover the operating range of the concentration C_A which is between $C_A^{min} = 0.1\,\text{mol/L}$ and $C_A^{max} = 0.5\,\text{mol/L}$. However, as discussed in Section 2, it is reasonable to allow elevated set-points in order to avoid overly conservative transitions toward the bounds of the concentration C_A. We introduce an elevation constant $w_{SP}^{elevation}$ and calculate the bounds of the set-point as:

$$w_{SP}^{max} = C_A^{max} + w_{SP}^{elevation}, \tag{17}$$

$$w_{SP}^{min} = C_A^{min} - w_{SP}^{elevation}. \tag{18}$$

We want to find a combination of β and $w_{SP}^{elevation}$ that (a) is feasible, that is, the filtered set-point can be tracked accurately without oscillations, and (b) allows for fast product transitions. In the following, we first present a routine to evaluate the feasibility and speed for a given combination of β and $w_{SP}^{elevation}$ and then explain how we explore the space of possible combinations.

To evaluate a combination of β and $w_{SP}^{elevation}$, we first optimize and then simulate all six possible transitions between the three product bands. Thus, each of the six transitions starts at a product p_i and ends at another product p_j, $i \neq j$. For a given combination of β and $w_{SP}^{elevation}$, we perform the following four steps for each transition:

1. As we assume that a fast transition is more critical than a slow one, we optimize a trajectory of set-points $w_{SP}(t)$ using model (i) to start from product p_i and reach the product band of product p_j as fast as possible. To generate this as-fast-as-possible set-point trajectory, we use exactly the same constraints as in the scheduling optimization. The resulting optimization problem reads:

$$\min_{w_{SP}(t)} \; -\sum_{t_0}^{t_f} z_{p_j}(t), \tag{19}$$

$$\text{s.t. } w_{SP,fil}(t) + 2\beta\frac{dw_{SP,fil}}{dt}\bigg|_t + \beta^2\frac{d^2w_{SP,fil}}{dt^2}\bigg|_t = w_{SP}(t) \quad \forall t \in [t_0, t_f], \tag{20}$$

$$w_{SP,fil}(t) - \left(C_{A,p_j}^{min} + \varepsilon_p\right) \geq -\left(1 - z_{p_j}(t)\right) \quad \forall t \in [t_0, t_f], \tag{21}$$

$$\left(C_{A,p_j}^{max} - \varepsilon_p\right) - w_{SP,fil}(t) \geq -\left(1 - z_{p_j}(t)\right) \quad \forall t \in [t_0, t_f], \tag{22}$$

$$C_A^{min} - w_{SP}^{elevation} \leq w_{SP}(t) \leq C_A^{max} + w_{SP}^{elevation} \quad \forall t \in [t_0, t_f], \tag{23}$$

$$w_{SP,fil}(t_0) = C_{A,p_i}, \tag{24}$$

$$\frac{dw_{SP,fil}}{dt}\bigg|_{t_0} = 0. \tag{25}$$

In Equations (19)–(25), $z_{p_j}(t)$ is a binary indicating if the filtered set-point $w_{SP,fil}$ has reached the band of the desired product p_j. Accordingly, $z_{p_j}(t)$ is 1 if $C_{A,p_j}^{min} + \varepsilon_p \leq w_{SP,fil}(t) \leq C_{A,p_j}^{max} - \varepsilon_p$ where ε_p is a small tolerance which we set equal to 0.003 mol/L. The value of $z_{p_j}(t)$ is enforced by Equations (21) and (22). Equation (20) is the SBM (i) and Equation (23) bounds the piece-wise constant set-point w_{SP}. Time discretization with collocation converts the dynamic optimization problem to an MILP.

2. We take the resulting set-point trajectory $w_{SP}(t)$ as input to a simulation of the set-point filter, the underlying PID-control, and the nonlinear process model.
3. Based on the simulation result, we check if the transition is feasible. We consider a transition to be feasible if (a) the concentration reaches the product band of the desired product p_j and (b) the concentration stays inside the band of p_j once this product band is reached.
4. We store the time needed to reach the product band Δt_s, which is calculated from the simulation result as the simulation gives the true closed-loop response.

A combination of β and $w_{SP}^{elevation}$ is considered feasible if all six transitions are feasible. We measure the quality of feasible parameter combinations by the sum of all six transition times, that is,

$$\Delta t_{\text{sum}} = \sum_{s \in \mathbb{S}} \Delta t_s, \tag{26}$$

where $\mathbb{S}$ is the set of possible transitions. As we aim for fast transitions, we prefer feasible combinations of β and $w_{\text{SP}}^{\text{elevation}}$ with a small value of Δt_{sum}.

To explore the space of possible combinations, we first set the set-point elevation to zero, that is, $w_{\text{SP}}^{\text{elevation}} = 0\,\text{mol/L}$, and start with $\beta = 0.1$ h. We increase β by steps of size $\Delta\beta = 0.01$ h and evaluate if all six product transitions are feasible. That is, for every value of β, we repeat steps 1–4 for all six transitions. The smallest time constant β for which all six transitions are feasible is $\beta^{\text{min}} = 0.26$ h. Starting from $\beta^{\text{min}} = 0.26$ h, we continue to increase β and additionally allow a set-point elevation. For every value of β, the set-point elevation $w_{\text{SP}}^{\text{elevation}}$ is increased by steps of size $\Delta w_{\text{SP}}^{\text{elevation}} = 0.01\,\text{mol/L}$ until one of the transitions becomes infeasible. That way, we find the highest possible set-point elevation for every β.

As Figure 5 shows, exploring the trade-off between set-point elevation and time constants improves the SBM performance significantly. The smallest, that is, fastest, possible time constant $\beta^{\text{min}} = 0.26$ h, which does not allow any set-point elevation, leads to a combined transition time of $\Delta t_{\text{sum}} = 6.23$ h. The slightly higher time constant $\beta = 0.36$ h in combination with a set-point elevation of $w_{\text{SP}}^{\text{elevation}} = 0.15\,\text{mol/L}$ allows to reduce the transition time by 35% to the optimum of $\Delta t_{\text{sum}} = 4.04$ h. The resulting transitions with the chosen optimal values are shown in Figure 6. Note that the set-point elevation is not strictly increasing with β due to the discretization. For example, with $\beta = 0.49$ h, a set-point elevation of $w_{\text{SP}}^{\text{elevation}} = 0.26\,\text{mol/L}$ is feasible, whereas for $\beta = 0.50$ h, $w_{\text{SP}}^{\text{elevation}} = 0.26\,\text{mol/L}$ is not feasible. The reason is that in one transition the set-point is at $w_{\text{SP}}^{\text{max}} = 0.76\,\text{mol/L}$ for one discretization time step longer with $\beta = 0.50$ h compared to $\beta = 0.49$ h leading to a slight overshoot of the concentration out of the product band.

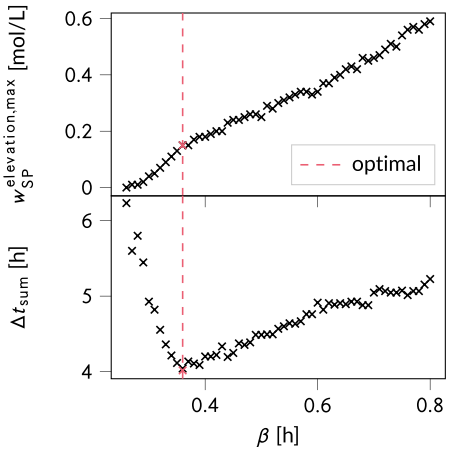

FIGURE 5 Result of the parameter tuning: maximum allowable set-point elevation $w_{\text{SP}}^{\text{elevation,max}}$ (top) and sum of all six transition times Δt_{sum} resulting with $w_{\text{SP}}^{\text{elevation,max}}$ (bottom) for different values of the time constant β. We choose the optimal, that is, smallest Δt_{sum} by setting $\beta = 0.36$ h and $w_{\text{SP}}^{\text{elevation}} = 0.15\,\text{mol/L}$.

3.2.2 | Energy demand model

As discussed in Section 2, model (ii) is needed in scheduling optimization to predict the process energy demand. In this case study, model (ii) needs to predict the cooling power Q_{cool} as a function of the controlled variable y_{cv}, which is the concentration C_A, and its time derivatives. Note that, in principle, the cooling power Q_{cool} is a process degree of freedom; however, the cooling power is set by the underlying PID-controller (Equation (14)). In scheduling optimization, the degree of freedom is the piece-wise constant set-point w_{SP} for the concentration C_A. This piece-wise constant set-point w_{SP} is filtered, resulting in a reference trajectory for both C_A and its time derivatives (compare to Figure 2). Thus, the data-driven energy demand model

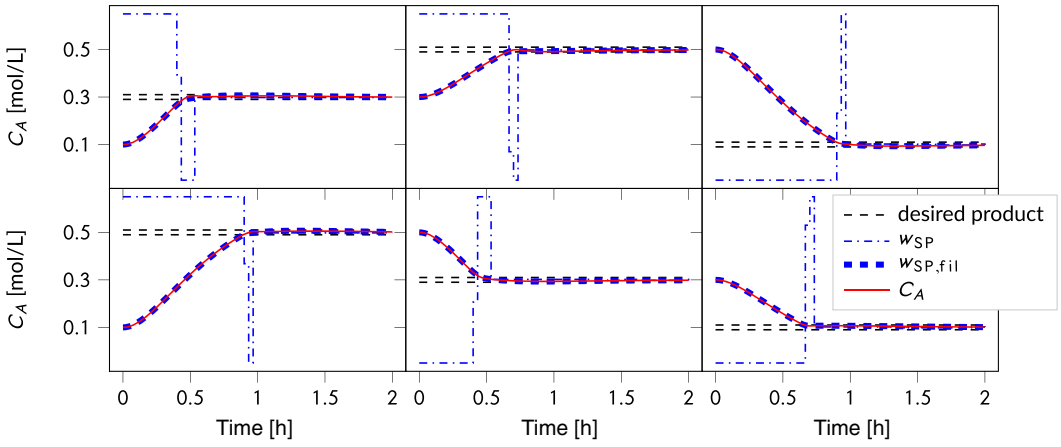

FIGURE 6 Six possible transitions between the three products with the chosen time constant $\beta = 0.36$ h and set-point elevation $w_{\text{SP}}^{\text{elevation}} = 0.15\,\text{mol/L}$ (compare to Figure 5). The piece-wise constant set-point from optimization w_{SP} results in a filtered set-point $w_{\text{SP,fil}}$, which can be tracked accurately such that the actual value of the concentration C_A resulting from the controlled nonlinear process model matches the filtered set-point $w_{\text{SP,fil}}$ well.

must approximate the response of the closed-loop system as a function of C_A and its time derivatives.

As the operation of the multiproduct reactor is divided in production and transition periods and we need to model the cooling power accurately in particular during the long production periods, we split Q_{cool} into a steady state and a dynamic part:

$$Q_{\text{cool}} = Q_{\text{cool}}^{\text{steady}} + Q_{\text{cool}}^{\text{dynamic}}. \tag{27}$$

To approximate the first contribution $Q_{\text{cool}}^{\text{steady}}$, we assume that steady-state cooling powers are known for all three products and interpolate $Q_{\text{cool}}^{\text{steady}}$ as a piece-wise affine function of C_A. The three steady-state operating points $C_A = \{0.1\,\text{mol/L}, 0.3\,\text{mol/L}, 0.5\,\text{mol/L}\}$ with corresponding cooling powers $Q_{\text{cool}}^{\text{steady}}$ lead to two piece-wise affine segments: the first affine segment approximates $Q_{\text{cool}}^{\text{steady}}$ for $C_A \le 0.3\,\text{mol/L}$ and the second affine segment approximates $Q_{\text{cool}}^{\text{steady}}$ for $C_A \ge 0.3\,\text{mol/L}$. With the binary variable $z_{\text{cool}}^{\text{steady}}$, we can express $Q_{\text{cool}}^{\text{steady}}$ as

$$\begin{aligned} Q_{\text{cool}}^{\text{steady}} = {} & Q_{\text{cool},0.3\,\text{mol/L}}^{\text{steady}} + m_1^{\text{steady}}\left(1 - z_{\text{cool}}^{\text{steady}}\right)(C_A - 0.3\,\text{mol/L}) \\ & + m_2^{\text{steady}} z_{\text{cool}}^{\text{steady}}(C_A - 0.3\,\text{mol/L}), \end{aligned} \tag{28}$$

where $Q_{\text{cool},0.3\,\text{mol/L}}^{\text{steady}}$ is the steady-state cooling power at $C_A = 0.3\,\text{mol/L}$, m_1^{steady} is the slope for $C_A \le 0.3\,\text{mol/L}$, and m_2^{steady} is the slope for $C_A \ge 0.3\,\text{mol/L}$. The slopes m_1^{steady} and m_2^{steady} are calculated from the cooling power at steady-state operating points (Table 1). The bilinear terms $z_{\text{cool}}^{\text{steady}} C_A$ are reformulated using the Glover reformulation.[40]

The approximation of $Q_{\text{cool}}^{\text{dynamic}}$ is fitted to simulation data. Again, we simulate all six possible transitions using the nonlinear reactor model and the underlying control. The resulting cooling power is the red curve in Figure 7. The total cooling power deviates from $Q_{\text{cool}}^{\text{steady}}$ (dashed green curve in Figure 7) during transitions. We model the dynamic part of the cooling power $Q_{\text{cool}}^{\text{dynamic}}$ as a linear function of the derivatives of the concentration, that is,

$$Q_{\text{cool}}^{\text{dynamic}} = c_1 \frac{dC_A}{dt} + c_2 \frac{d^2 C_A}{dt^2}, \tag{29}$$

with the two fitting parameters c_1, c_2, whose values are determined using the normal equation method.[41] The values are: $c_1 = -3.10\,\text{MJL/mol}$, $c_2 = 0.444\,\text{MJLh/mol}$. The resulting approximation of Q_{cool} is shown in blue in Figure 7. Note that in Figure 7, the concentration does not reach steady state after entering the product bands. Still, the fitted dynamic cooling power $Q_{\text{cool}}^{\text{dynamic}}$ is negligible for five of six production phases and only in the second production phase a small offset between model and actual cooling power occurs. The purely linear model in Equation (29) is the simplest possible choice to model the dynamic part and already leads to satisfying results. In case study 3, a more complex model accounting for internal process states is demonstrated.

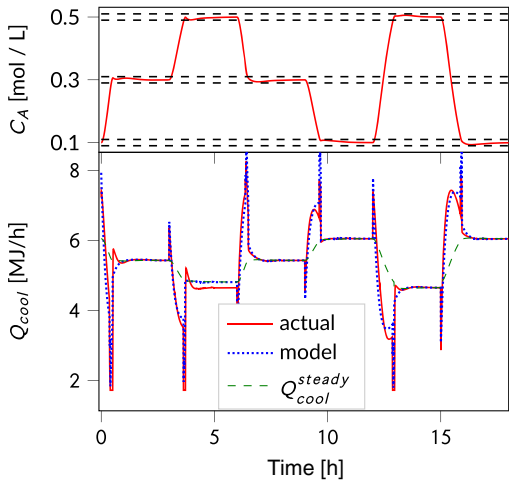

FIGURE 7 Fitting results for steady state and total cooling power $Q_{\text{cool}}^{\text{steady}}$ and Q_{cool}, respectively, of the process energy demand model (compare to Equations (27) and (28))

3.2.3 | Energy system model

For the energy system model (iii), we have to calculate the electric input power $P_{\text{CC},i}$ needed for the compression chillers as a function of the required cooling power $Q_{\text{CC},i}$. As the COP of the compression chillers depends on the part-load fraction (Equation (13)), $P_{\text{CC},i}$ is a nonlinear function of $Q_{\text{CC},i}$, which we approximate as a piece-wise affine function. We use two piece-wise affine segments per chiller with the breakpoint at 70% part load; two segments provide a good approximation.[7] The piece-wise affine curves can be modeled without introduction of additional binary variables, as the electric input power $P_{\text{CC},i}$ is a convex function of the cooling power $Q_{\text{CC},i}$. Using equations from Neisen et al.,[42] we introduce two continuous variables $y_{i,1}$, $y_{i,2}$ that cover the two affine segments:

$$Q_{\text{CC},i} = y_{i,1} + y_{i,2} \quad \forall i = 1,2,3, \tag{30}$$

$$P_{\text{CC},i} = P_{\text{CC},i}^{\min} z_{\text{on,CC},i} + y_{i,1} m_{i,1} + y_{i,2} m_{i,2} \quad \forall i = 1,2,3. \tag{31}$$

In Equation (31), $P_{\text{CC},i}^{\min}$ is the electric input power at minimum part-load of chiller i, $z_{\text{on,CC},i}$ is a binary indicating whether chiller i is active, and $m_{i,1}$, $m_{i,2}$ are the slopes within the two piece-wise affine segments. Finally, we include the energy balance stating that the cooling demand of the reactor must be matched by the compression chillers:

$$\sum_{i=1}^{3} Q_{\text{CC},i} = Q_{\text{cool}}. \tag{32}$$

Further details on the scheduling optimization problem such as discretization and problem-specific constraints are given in the Supporting Information.

3.3 | Sequential steady-state scheduling benchmark

This benchmark represents a typical sequential scheduling without DR, referred to as SEQ in the following. First, the process schedule is optimized with only the product revenue $\Phi_{Product}$ in the objective function. Second, the energy costs are minimized for fixed production decisions. Detailed information are given in the Supporting Information.

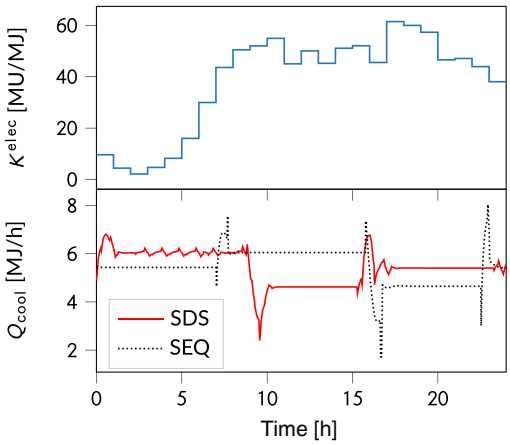

FIGURE 8 Electricity price K^{elec} and simulated cooling power Q_{cool} for *simultaneous dynamic scheduling* (SDS) and sequential steady-state scheduling (SEQ). SDS performs demand response and shifts cooling power to times of favorable prices.

3.4 | Scheduling with full nonlinear model

To estimate an upper bound on the economic performance of simultaneous scheduling, we perform an optimization with the nonlinear full-order system model. To this end, we replace the models (i), (ii), (iii) in the optimization problem with the nonlinear reactor model (Equations (11) and (12)) and the nonlinear compression chiller efficiency (Equation (13)). Again, time is discretized using collocation and we receive an MINLP. We solve the MINLP optimization problem using BARON version 21.1.13[43] in heuristic mode, that is, the resulting solution is no rigorous bound. We refer to this benchmark as MINLP. To obtain a feasible initial point, we fix the binary variables to the values resulting from our SDS and solve the resulting NLP.

3.5 | Results

In this section, we compare the economic profit obtained with our SDS to the sequential scheduling (SEQ) and the full-order nonlinear scheduling (MINLP). While in case of the MINLP the profit is the objective value in the optimization, for the sequential scheduling and the SDS, the profit is derived from a simulation of the original nonlinear process model. Accordingly, the optimized set-point sequence is used as input to a simulation of the underlying controller and the nonlinear process model.

The MINLP solution improves the SEQ solution by 5.5%. Our SDS gains 5.2% compared to SEQ and thus captures 95% of the MINLP improvement. The improved economics mainly stem from DR, that is, products with higher cooling demands are produced at times

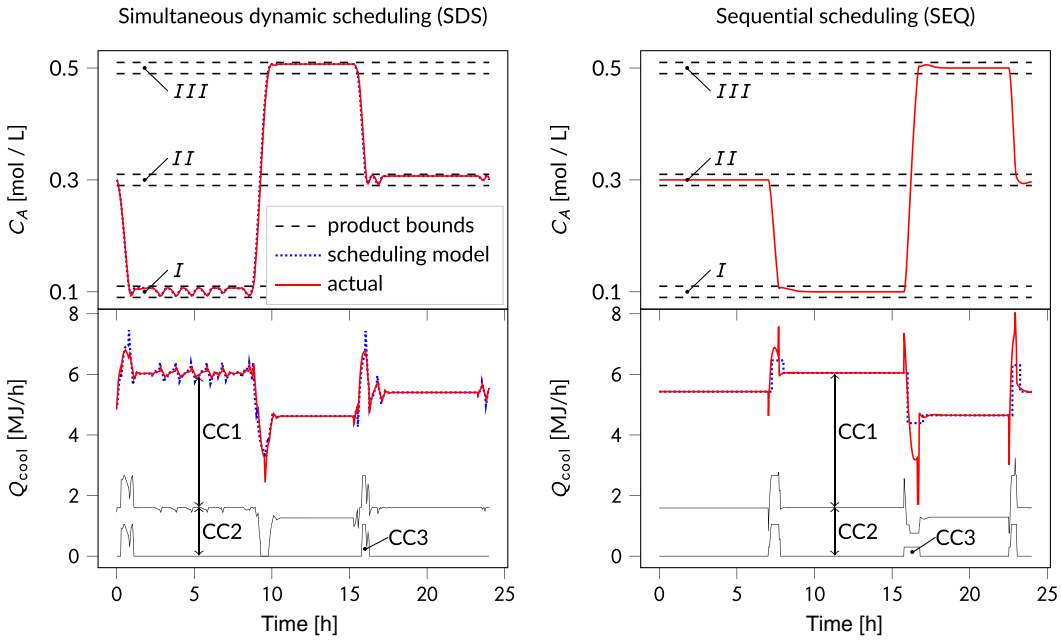

FIGURE 9 Comparison of concentration C_A and cooling power Q_{cool} between simultaneous dynamic scheduling (SDS, left) and sequential scheduling (SEQ, right). We indicate the three product bands (*I*, *II*, *III*) and the fraction of the cooling power Q_{cool} that is supplied by the three compression chillers (CC1, CC2, CC3).

of lower electricity prices (Figure 8). Additionally, we notice a higher energy efficiency during transition phases such that our SDS reduces the amount of electricity consumed by 1.2% compared to SEQ.

Figure 9 shows concentration C_A and cooling power Q_{cool} for both SDS and SEQ. In the case of SDS, the difference between the optimization model and the actual cooling power during the transitions is smaller than in the case of SEQ because the dynamics of the cooling power are modeled in SDS while SEQ only considers the average cooling power during a transition. Modeling the dynamics of the cooling power within a transition leads to better scheduling decisions regarding the on/off status of the three compression chillers. The most distinct difference occurs in the transition from product *I* to product *III*. In the sequential scheduling, this transition features a high cooling power peak, which requires to turn on chiller 3 with the worst COP. In the case of SDS, the same transition is shaped such that it is not necessary to turn on chiller 3. Moreover, SDS anticipates that chiller 2 with the medium COP can be turned off during the second half of the transition. We expect that energy efficiency improvements are even higher in cases with longer transitions. Naturally, the potential for energy efficiency improvements depends on the accuracy of the data-driven energy demand model (ii).

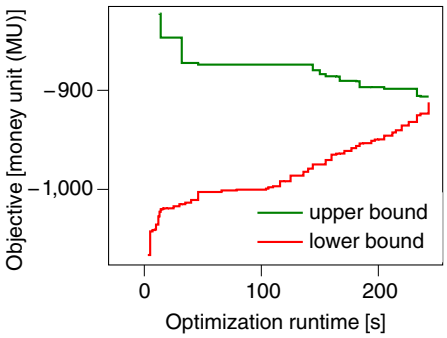

FIGURE 10 Convergence plot of *simultaneous dynamic scheduling*

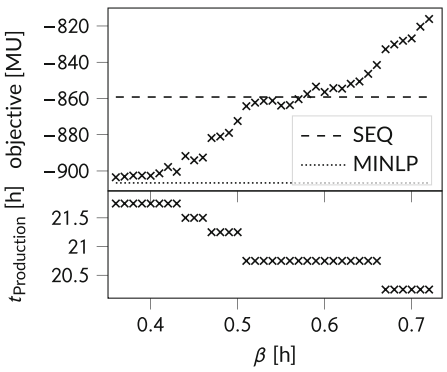

FIGURE 11 Objective (in money unit [MU]) and total production time $t_{Production}$ for different time constants β starting from nominal $\beta = 0.36$ h up to $\beta = 0.72$ h. The objective values resulting from the sequential approach (SEQ) and MINLP optimization with both 21.75 h of production are shown for comparison (dashed and dotted lines, respectively).

Note that in our illustrative example, we assume that once the energy system components are active they can react instantaneously. Moreover, we assume that the frequency of on/off-switches resulting from the scheduling optimization with 15 min resolution for discrete variables is acceptable. In practice, it might be necessary to consider ramp limits,[22] or minimum up and down times.[20] Such constraints can be added in a straightforward manner to the formulation if needed.

A solution with a 1.0% optimality gap is found and proven in 244 s. Such a solution time is applicable for both offline day-ahead scheduling and online re-scheduling during the day, for example, with a sampling time of 1 h. Note that in re-scheduling the solution from the last scheduling-iteration can be used for initialization to further speed up the optimization. We also observe that SDS finds good feasible solutions quickly as shown in the convergence plot (Figure 10). After 32 s, a solution is found that has only 4.4% gap to the final lower bound and already outperforms the sequential scheduling.

3.5.1 | Influence of time constant β

If a nonlinear process model is not available, the time constant β cannot be chosen as in this case study but needs to be chosen based on intuition or recorded product transitions. In result, the time constant might be suboptimal. To study the influence of the time constant choice on the profit, the time constant in our case study is increased from the optimal value $\beta = 0.36$ h by up to 100% (Figure 11). Note that the profit is calculated in a simulation using the original process model which leads to small differences between scheduling optimization and process simulation and therefore the simulated objective shown in Figure 11 does not strictly increase with β.

We find that as long as β is increased by 20% or less the objective does not worsen more than 0.5%. This result can be explained by the total production time which is 21.75 h for $\beta = 0.36$ h. These 21.75 h of production are still reached for $\beta = 0.43$ h and the loss in profit is small. Generally, production time changes in 0.25 h steps corresponding to the time discretization of the binary variables (compare to the Supporting Information). When β is increased by more than 20% above the optimal value, production is lost and the objective substantially worsens. But, even for a 50% increase, the objective is still better than that of the sequential solution.

4 | CASE STUDY 2: REACTOR WITH VARIABLE CONCENTRATION

While multi-product processes are one example for scheduling-relevant dynamics, single-product processes can also introduce dynamics if they can vary their controlled variable around a nominal value as long as the nominal value is reached on average over the considered time horizon. To demonstrate that our SDS also works for a single-product case, we present a second case study and again study the influence of the time constant. The second case study is constructed by modifying the first one.

4.1 | Setup

A similar setup is used as in the previous case study with a CSTR and three compression chillers (Figure 4). Instead of a multi-product CSTR, we assume a single-product CSTR with a nominal concentration $C_A^{\text{nom}} = 0.3\,\text{mol/L}$. The CSTR has flexibility because we assume that the concentration is allowed to vary between $C_A^{\text{min}} = 0.09\,\text{mol/L}$ and $C_A^{\text{max}} = 0.51\,\text{mol/L}$ as long as the nominal concentration is reached on average over the time horizon $t_f - t_0$. Accordingly, the condition

$$\int_{t_0}^{t_f} C_A dt = C_A^{\text{nom}}(t_f - t_0) \tag{33}$$

has to hold. Such setups occur when the product can be stored and is well-mixed in the storage tank. Note that an equation of this type would also occur for processes having a variable production rate as controlled variable y_{cv}. Only the concentration C_A in Equation (33) would have to be replaced by the production rate.

Obviously, it is favorable to operate at concentrations with a high cooling demand at times of low electricity prices and at concentrations with low cooling demand at times of high prices. The challenge for scheduling optimization thus is to find a trajectory for the concentration that (a) can be realized by the process and (b) reaches the nominal concentration on average. At the same time, the on/off status of the chillers has to be determined. Note that the scheduling problem has three differences compared to the previous case:

1. Only the cumulative energy costs at final time $\Phi_{\text{Energy}}(t_f)$ are considered in the objective (Equation (4)) since the production volume is fixed.
2. All constraints associated with the different products and the production bands are removed (Equations (S1), (S2), (S6)–(S10)).
3. Equation (33) is included such that the nominal concentration is reached on average.

As energy costs are the only objective function in the second case study, a sequential scheduling is not applicable because there is no objective for the process optimization. Thus, we benchmark our SDS against a steady-state operation of the CSTR at the nominal concentration. Again, as a second benchmark, an MINLP optimization is performed using BARON in heuristic mode. A feasible initial point is found by fixing the binary variables to the values from our SDS and solving the resulting NLP.

4.2 | Results

The MINLP solution improves the steady-state solution by 6.7%. Our SDS reduces costs by 5.5% compared to the steady-state benchmark and thus captures 82% of the MINLP improvement. The optimization runtime of our SDS approach is only 55 s. Note that again the MINLP optimization with BARON does not provide a feasible point without initialization from the SDS solution.

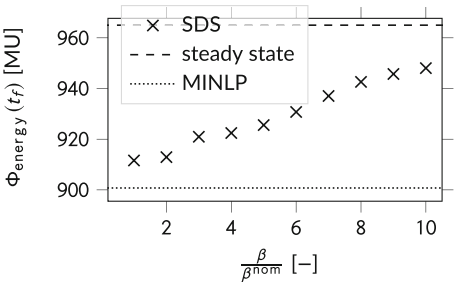

FIGURE 12 Energy costs $\Phi_{\text{energy}}(t_f)$ (in money unit [MU]) in the second case study achieved with simultaneous dynamic scheduling (SDS) for different time constants β normalized to nominal value $\beta^{\text{nom}} = 0.36$ h. The energy costs resulting from steady-state operation and the MINLP benchmark are shown for comparison (dashed and dotted lines, respectively).

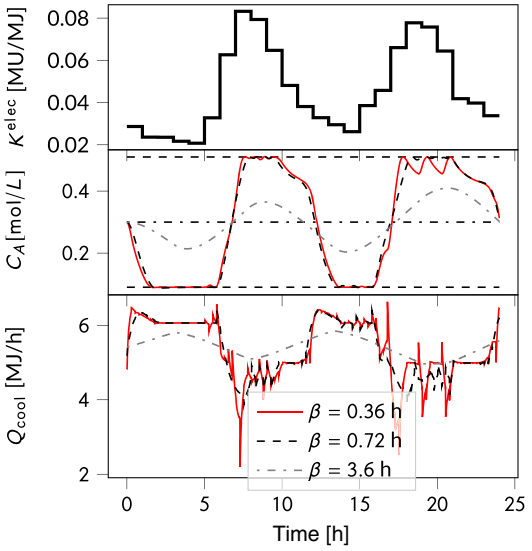

FIGURE 13 Electricity price K^{elec}, concentration C_A, and cooling power Q_{cool} in the second case study for three values of the time constant β

Compared to case study 1, the choice of the time constant β has a much lower impact on the economic result (Figure 12). Note that we use the same time constant β as in case study 1, because the transitions studied during tuning cover the complete range of allowed concentrations. If β is doubled from 0.36 to 0.72 h, the cost reduction still amounts to 5.4% compared to steady-state operation (Figure 12). The operation is very similar for both time constants and the cooling power only deviates significantly in hours 1, 6–7, 11, and 16–17 (Figure 13). In hours 16 and 17, the schedule with $\beta = 0.72$ h drives the reactor from minimum concentration to maximum concentration. The higher flexibility of the low time constant $\beta = 0.36$ h allows to consume more cooling in hour 16 and less in hour 17 compared to the case where $\beta = 0.72$ h. Still, the larger time constant can capture the main trend of the electricity price profile, which has a peak in the morning and another one in the afternoon. Such a price profile is typical for the German market where the main price periodicities are 24 and 12 h.[38] Even if β is increased by a factor of 10, the scheduling

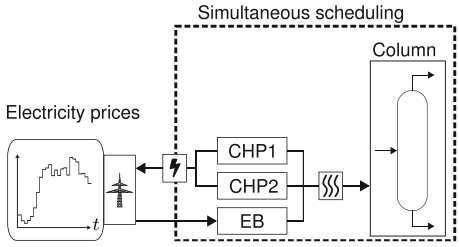

FIGURE 14 Case study 3: simultaneous scheduling of a distillation column heated by two combined heat and power plants (CHP1, CHP2) and a electricity-driven boiler (EB). Time-varying electricity prices provide an economic incentive for DR.

can still capture the main trend of the electricity price profile (Figure 13). Therefore, significant cost reductions can be reached even if the chosen time constants are far above the optimal value.

5 | CASE STUDY 3: DISTILLATION COLUMN WITH VARIABLE PURITY

In this section, we study a case similar to the second case but, instead of a SISO CSTR, we consider a distillation column as a MIMO process. The purity of both top and bottom product can be varied throughout the day as long as the desired purity is reached on average.

5.1 | Setup

The heat demand of a distillation column is satisfied by two CHPs and an EB (Figure 14). Electricity produced by the CHPs is sold to the electricity grid. For the distillation column, we use a generic benchmark model of a binary distillation proposed by Skogestad and Morari[44] together with a liquid flow model from Skogestad et al.[45] The column model consists of $N + 1$ mass balances of the light boiling component and $N + 1$ mass balances of the liquid hold-ups where $N = 40$ is the number of theoretical trays. In total, the column model has 82 differential states. It is assumed that the heat demand of the column is proportional to the boilup flow rate V and the heat demand is scaled such that the column requires 1 MW of heating in nominal operation. The two CHPs have 800 and 500 kW nominal thermal power and are subject to 50% minimum part-load constraints.[7] The EB has 800 kW nominal power and a 20% minimum part-load constraint.[46] Further details on the distillation model and the CHP and EB models are given in the Supporting Information.

For the column, the feed flow F is fixed by an upstream process. Four flows can be manipulated: the reflux flow rate L, the boilup flow rate V, the distillate flow rate D, and the bottom flow rate B. Accordingly, the vector of manipulated variables is

$$\mathbf{u} = \begin{pmatrix} L \\ V \\ D \\ B \end{pmatrix}. \tag{34}$$

The variables to be controlled are the vapor mole fraction of the light component entering the condenser y_D, its liquid mole fraction in the bottom flow x_B, the condenser hold-up M_D, and the condenser hold-up M_B:

$$\mathbf{y}_{\text{cv}} = \begin{pmatrix} y_D \\ x_B \\ M_D \\ M_B \end{pmatrix}. \tag{35}$$

We couple the mole fractions y_D and x_B with each other by defining the purity ρ which is equal to y_D and $1 - x_B$. The coupling $y_D = 1 - x_B$ can be applied in this case study, as the feed purity z_F is 50% and in steady-state both bottom flow rate B and the distillate flow rate D are equal to 50% of the feed flow rate F. A more general case is discussed in the Supporting Information.

The hold-ups M_D and M_B shall be maintained constant at their nominal values M_D^{nom} and M_B^{nom} irrespective of the current purity ρ. Accordingly, the vector of filtered set-points $\mathbf{w}_{\text{SP,fil}}$ can be given as a function of the filtered purity set-point $\rho_{\text{SP,fil}}$:

$$\mathbf{w}_{\text{SP,fil}}(\rho_{\text{SP,fil}}) = \begin{pmatrix} \rho_{\text{SP,fil}} \\ 1 - \rho_{\text{SP,fil}} \\ M_D^{\text{nom}} \\ M_B^{\text{nom}} \end{pmatrix}. \tag{36}$$

The purity ρ can be varied between $\rho^{\text{min}} = 0.85$ and $\rho^{\text{max}} = 0.95$ as long as the nominal value $\rho^{\text{nom}} = 0.9$ is reached on average.

To this end, we use two PI controllers[31] to control the mole fractions y_D and x_B by manipulating the flow rates L and V, respectively. Further details are given in the Supporting Information. For the hold-ups M_D^{nom} and M_B^{nom}, we do not model the controllers explicitly but follow the common assumption that an underlying control sets the flows D and B such that the hold-ups are controlled perfectly.[44]

With this case study, we demonstrate that a MIMO process does not necessarily lead to a MIMO SBM (cf., discussion in Section 2). Instead, controlled variables such as the mole fractions y_D and x_B can be given as functions of a single scheduling-relevant variable such as the purity ρ here. At the same time, other controlled variables, such as the hold-ups M_D, M_B, need to be maintained constant irrespective of the scheduling-relevant variable. As a consequence, instead of four SBMs only one SBM describing the dynamics of the purity ρ is needed.

5.2 | Simultaneous dynamic scheduling

In this section, we develop the three parts of our model.

For the scale-bridging production process model (i), a first-order model is chosen because all four controlled variables in $\mathbf{y}_{\text{cv}}$ can be controlled with a relative degree $r = 1$ (cf. differential model equations in the Supporting Information). Thus, model (i) for the filtered purity set-point $\rho_{\text{SP,fil}}$ is

$$\rho_{\mathrm{SP,fil}} + \tau \frac{d\rho_{\mathrm{SP,fil}}}{dt} = \rho_{\mathrm{SP}}, \tag{37}$$

with one time constant τ that must be tuned. For the tuning, a similar procedure as in the previous case studies is applied. Again, we study six representative transitions. The aim is to find a time constant τ and set-point bounds $\rho_{\mathrm{SP}}^{\min}$, $\rho_{\mathrm{SP}}^{\max}$ that give fast transitions. At the same time, deviations between y_D and $\rho_{\mathrm{SP,fil}}$ and between x_B and $1-\rho_{\mathrm{SP,fil}}$ need to be within a certain tolerance. Details on the tuning are given in the Supporting Information. The resulting values are $\tau = 10$ min, $\rho_{\mathrm{SP}}^{\min} = 0.8485$, $\rho_{\mathrm{SP}}^{\max} = 0.9515$.

For the energy demand model (ii), we split the vapor flow V into a steady-state and a dynamic part (compare to Equation (27)), that is,

$$V = V^{\mathrm{steady}} + V^{\mathrm{dynamic}}, \tag{38}$$

where V^{steady} is modeled as a piece-wise affine function with two segments of the purity ρ because the vapor flow V in steady state is a nonlinear function of the purity. The dynamic part V^{dynamic} is approximated by a linear model with the derivative of the scale-bridging variable, $\frac{d\rho_{\mathrm{SP,fil}}}{dt}$, as input. However, in contrast to Equation (29), the model for V^{dynamic} features an internal state x_{int} and is given by

$$\frac{dx_{\mathrm{int}}}{dt} = a x_{\mathrm{int}} + b \frac{d\rho_{\mathrm{SP,fil}}}{dt}, \tag{39}$$

$$V^{\mathrm{dynamic}} = c x_{\mathrm{int}} + d \frac{d\rho_{\mathrm{SP,fil}}}{dt}, \tag{40}$$

with fitting coefficients a, b, c, d that are fitted to the simulated transitions that result from the tuning of model (i) discussed above. The rational for including an internal state x_{int} is shown in Figure 15 where one transition is visualized: after 15 min, the filtered purity set point $\rho_{\mathrm{SP,fil}}$ has reached the steady-state value, that is, $\rho_{\mathrm{SP}} = \rho_{\mathrm{SP,fil}}$ and $\frac{d\rho_{\mathrm{SP,fil}}}{dt} = 0$. However, the vapor flow V is not in steady state because the uncontrolled states inside the column are not in steady state and it takes roughly another 15 min until steady state is reached. The fitting constant $a = -0.14\,\frac{1}{\mathrm{min}}$ corresponds to a time constant of 7.1 min and represents internal dynamics of the column. We also studied energy demand models with more than one internal state but did not find significant improvements compared to the one with a single internal state (Equation (39)).

With this third case study, we demonstrate the model-order reduction capabilities of SBMs and data-driven models. The 82 differential states of the full-order column model are reduced to just 2 states: the filtered purity set-point $p_{\mathrm{SP,fil}}$ and the internal state of the energy demand model x_{int}.

In the energy system model (iii), the part-load behavior of the CHPs is modeled with one piece-wise affine segment leading to a reasonable discretization.[7] For the EB, a constant efficiency is assumed.[47]

We use a quarter-hourly electricity price profile because $\Delta t_{\mathrm{elec}} = 15$ min being similar to the time constant of the SBM

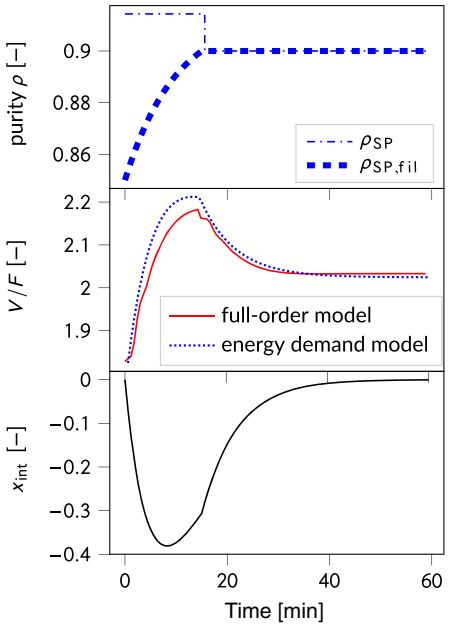

FIGURE 15 Exemplary transition showing purity set-point ρ_{SP} and filtered set-point $\rho_{\mathrm{SP,fil}}$ (top), reboiler flow V normalized to the feed flow F calculated from full-order model and energy demand model (Equations (38) and (40)) (middle), and the internal state x_{int} of the energy demand the model calculated based on Equation (39) (bottom)

($\tau = 10$ min) presumably causes more pronounced dynamic operation than in the previous case studies. The price profile is taken from the German intra-day market and occurred on January 13, 2021.[48] A discretization with $\Delta t_{\mathrm{cont}} = 15$ min and $N_{\mathrm{cp}} = 3$ collocation points is used. As the 15-min price profile causes excessive on–off switching of the energy system components in preliminary investigations, we require a minimum up-time of 1 h and a minimum down-time of 1 h for all three energy system components. Such constraints are often used in energy system optimization as excessive on–off switches often have negative effects on component life-time.[20] The scheduling optimization problem is solved with Gurobi 9.1.2[49] on the same machine as before. Again we use a 1% optimality gap.

5.3 | Benchmarks

We consider two benchmarks, a steady-state operation at nominal purity and a sensitivity analysis where we halve the nominal time constant $\tau = 10$ min. The latter leads to operations with time constants that render some transitions infeasible but allows us to estimate the performance lost by the scale-bridging approach in comparison to an optimization with the original full-order nonlinear process model that, unlike the SBM, would not be limited by the slowest transition. We perform this sensitivity analysis with smaller time constants since an optimization with the full-order process model in this case study would be too computationally challenging due to the large scale of the MINLP.

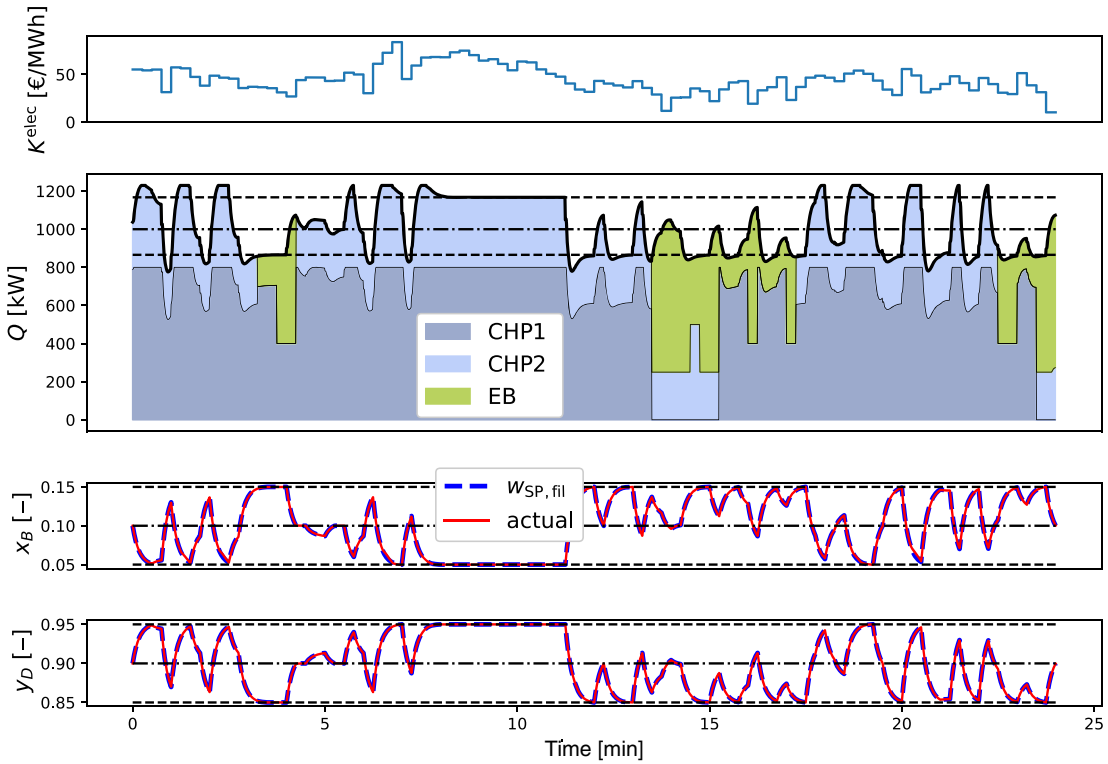

FIGURE 16 Resulting operation for the third case study. Top: electricity price K^{elec}. Center: heat demand Q of the column (bold black line) together with nominal value (dashed dotted line) and minimum and maximum steady-state heat demands (dashed lines). The portions of the heat demand supplied by the two combined heat and power plants (CHP1 and CHP2) and the electricity-driven boiler (EB) are indicated with colors. Bottom: actual values of bottom composition x_B and top composition y_D together with their respective filtered set-points $w_{SP,fil}$

5.4 | Results

Our SDS reduces costs by 4.3% compared to a steady-state operation whose results are shown in Figure S3. The SDS optimization converges to the pre-defined optimality gap of 1% within 125 s. Like in the previous case studies, near-optimal feasible points are found even faster (cf. Figure S4).

The resulting operation with the nominal time constant $\tau = 10$ min is shown in Figure 16. Due to the 15-min price profile, the operation is more dynamic than in the previous case studies. The column is only operated in steady state between $t = 3.5$ h and $t = 4$ h and between $t = 8.25$ h and $t = 11.25$ h. Still, the PI controllers track the filtered set-point accurately for both mole fractions x_B and y_D (Figure 16). The average mole fractions in the storage after the 1 day scheduling time horizons are:

$$x_D^{average} = \frac{\int_{t=0h}^{t=24h} x_D Ddt}{\int_{t=0h}^{t=24h} Ddt} = 0.90040 > \rho^{nom} = 0.9, \quad (41)$$

$$x_B^{average} = \frac{\int_{t=0h}^{t=24h} x_B Bdt}{\int_{t=0h}^{t=24h} Bdt} = 0.09967 < 1 - \rho^{nom} = 0.1. \quad (42)$$

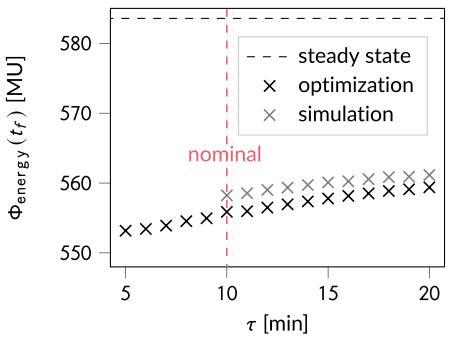

FIGURE 17 Energy costs $\Phi_{energy}(t_f)$ (in money unit [MU]) in the third case study achieved with different time constants τ. The energy costs resulting from steady-state operation are shown for comparison.

Thus, both top and bottom product stream achieve the desired purity on average.

Figure 16 shows that the optimization seeks to operate the column at high purities and high heat demands at times of high prices (e.g., hour 20–20.5). By supplying the required heat from the CHPs, electric power can be sold to the market at a high price. However, also at times of low electricity prices, a comparatively high heat demand can be seen (e.g., hour 13.75–14.25 or 16–16.25). Here, the EB is operated close to its maximum load because electricity is cheap. Only

at times of medium prices, the column is operated at low purities resulting in a low heat demand (e.g., hour 3.25–4). These interactions between the purity of the column and the on/off-status of energy system components demonstrate the advantages of a simultaneous scheduling of process and energy system.

In Figure 17, the sensitivity of the energy costs with respect to the time constant τ is shown. For time constants above the nominal value, the optimized energy costs are compared to simulated energy costs. The energy costs obtained in the simulation are always slightly higher than those predicted by the optimization due to inaccuracies of the data-driven energy demand model (ii). Comparing different time constants, we can conclude that the sensitivity toward the time constant is relatively weak. For instance, when the time constant is doubled from $\tau = 10$ min to $\tau = 20$ min, the simulated energy costs only increase by 0.5%.

To estimate the performance lost due to the conservatism of the scale-bridging approach, we halve the nominal time constant $\tau = 10$ min and study the resulting optimized energy costs. Note that this yields a lower bound for the energy costs as some transitions are not feasible for the halved time constant $\tau = 5$ min. However, this lower bound is only 0.5% smaller than the optimized energy costs with the nominal time constant (Figure 17). Thus, the 4.3% cost reduction achieved by our SDS approach already realizes most of the overall DR potential while being able to run within 5 min. We therefore conclude that SDS offers a favorable compromise between solution quality and optimization runtime.

6 | CONCLUSION AND DISCUSSION

For power-intensive processes, volatile electricity prices provide an opportunity to increase profit via DR. A particularly promising DR option is the simultaneous scheduling optimization of processes and their energy systems. As such an optimization must consider scheduling-relevant process dynamics as well as on/off-decisions in the energy supply system, computationally challenging nonlinear mixed-integer dynamic optimization (MIDO) problems arise. In this work, we present an efficient SDS approach that relies on a tailored scheduling model consisting of (i) a linear SBM for the closed-loop response of the process, (ii) a data-driven model for the process energy demand, and (iii) a mixed-integer linear programming (MILP) model of the energy system. Using a discrete time formulation and collocation, we receive an overall MILP formulation that can be optimized in practically relevant times.

First, we apply the method to a case study of a multiproduct CSTR cooled by three compression chillers. Compared to a typical sequential scheduling, we find that the presented SDS approach improves economic profit by 5.2%, just shy of the 5.5% found by nonlinear scheduling optimization using the original nonlinear process model. Second, we investigate a single-product reactor with a variable concentration. Here, SDS outperforms a steady-state operation by 5.5% while a nonlinear scheduling reaches 6.7%. Third, we investigate a distillation column heated by two CHPs and an EB. The distillation column is a 4×4 MIMO process; however, one SBM is sufficient as we couple top and bottom purity and hold condenser and reboiler hold-up constant irrespective of the purity. We thereby demonstrate the model-order reduction potential of our approach driving down the number of states from 82 to 2. Cost reduction of 4.3% compared to steady-state operation is achieved.

In all three case studies, the optimization runtime is sufficiently fast for online optimization. As the proposed scheduling model always has the same basic structure, we expect the method to be real-time applicable in many cases.

A restriction of our method is that the scale-bridging approach imposes a single common linear closed-loop response in all operating regimes, which may cut off some of the process flexibility and thus DR potential. For example, in our first case study, we must choose the time constants of the enforced linear closed-loop response such that all six product transitions are feasible. Due to the nonlinear behavior of the CSTR, some of the transitions could in principle be performed faster; however, the critical transition, that is, the slowest one, limits the time constants for the SBM. Moreover, it may in general be difficult to find the time constants that give the fastest possible linear closed-loop response. Finding the time constants using the heuristic used in our case studies is straightforward if the controlled process can be simulated and the relevant transitions can be studied in numerical experiments. If several controlled variables should be varied independently of each other, the combinatorial complexity of the heuristic procedure would increase as more than one SBM would be needed. Then, it might no longer be possible to simply sample the space of possible combinations but some kind of black-box optimization may be required. For multi-product processes, which are inherently dynamic, the time constants can also be chosen based on recorded transitions. Our sensitivity study shows that, as long as transition times are only moderately larger than necessary, costs can still be reduced compared to a standard sequential scheduling. For processes that are currently operated in steady state without DR, no recorded transitions might be available. However, we demonstrate that, for such processes, time constant choice is less critical as even greatly suboptimal values may allow to follow slow trends in the electricity price profile.

Overall, our results demonstrate that the proposed method offers a favorable trade-off between accurate handling of dynamic flexibility and online applicable optimization run-times.

NOMENCLATURE

Abbreviations

CC	compression chiller
CHP	combined heat and power plant
COP	coefficient of performance
CSTR	continuous stirred tank reactor
DR	demand response
EB	electricity-driven boiler
KKT	Karush-Kuhn-Tucker
MIDO	mixed-integer dynamic optimization
MILP	mixed-integer linear programming

MIMO	multiple input multiple output
MINLP	mixed-integer nonlinear programming
MPC	model predictive control
MU	money unit
PID	proportional–integral–derivative
PI	proportional–integral
SBM	scale-bridging model
SDS	simultaneous dynamic scheduling
SEQ	sequential scheduling benchmark
SISO	single-input single-output
SO-MPC	scheduling-oriented model predictive control

Greek symbols

β	time constant of natural oscillation
ε	safety margin
ζ	damping coefficient
ϱ	density
ρ	scheduling-relevant variable
τ	time constant
$\overline{\tau}$	scaled time
Φ	objective

Latin symbols

A–**H**	matrices
a, b, c, d	fitting coefficients
B	bottom flow rate
C_A	concentration of component A
c_P	heat capacity
D	distillate flow rate
E_A	activation energy
F	feed flow rate
f, g	functions
f_e	finite element
ΔH_r	enthalpy of reaction
K	price
K_P	proportional controller constant
k	reaction constant
L	reflux flow rate
l	Lagrange polynomial
M_k	hold-up of tray k
m	linear slope
N	number of trays
N_{cp}	order of collocation polynomial
n	natural number
P	power
Q	thermal power
q	flow rate
R	gas constant
r	order of differential equation
T	temperature
t	time
u	manipulated variable
V	volume (case study 1 and 2) or boilup flow rate (case study 3)
w_{SP}	set-point
x	differential state
x_k	liquid mole fraction on tray k
y	continuous variable
y_k	vapor mole fraction on tray k
z	discrete variable

Sets

$\mathbb{E}$	end-energy forms
$\mathbb{P}$	products
$\mathbb{S}$	set of possible transitions
$\mathbb{T}_{dis}$	timepoints on discrete grid

Subscripts

0	initial
B	reboiler
c	component
cv	controlled variable
cont	continuous
cool	cooling
D	condenser
dis	discrete
e	end-energy form
ec	energy costs
ed	energy demand
elec	electricity
f	final
f_e	finite element
fil	filtered
I	integral
in	input
int	internal
on	on–off status
out	output
p	product
s	transition
SP	set point
sum	summed value

Superscripts

end	final value
elec	electricity
max	maximum value
min	minimum value
nom	nominal
start	starting value
steady	steady-state value

AUTHOR CONTRIBUTIONS

Florian Joseph Baader: Conceptualization (lead); investigation (lead); methodology (lead); software (lead); validation (lead); visualization

(lead); writing – original draft (lead). **André Bardow:** Conceptualization (supporting); funding acquisition (lead); supervision (equal); writing – review and editing (supporting). **Manuel Dahmen:** Conceptualization (supporting); supervision (equal); writing – review and editing (lead).

ACKNOWLEDGMENTS

This work was supported by the Helmholtz Association under the Joint Initiative "Energy System 2050 – A Contribution of the Research Field Energy" and under the Initiative "Energy System Integration." Open Access funding enabled and organized by Projekt DEAL.

DATA AVAILABILITY STATEMENT

Data sharing not applicable to this article.

ORCID

Florian Joseph Baader https://orcid.org/0000-0002-8434-4438
André Bardow https://orcid.org/0000-0002-3831-0691
Manuel Dahmen https://orcid.org/0000-0003-2757-5253

REFERENCES

1. Merkert L, Harjunkoski I, Isaksson A, Säynevirta S, Saarela A, Sand G. Scheduling and energy – industrial challenges and opportunities. *Comput Chem Eng*. 2015;72:183-198.
2. Mitsos A, Asprion N, Floudas CA, et al. Challenges in process optimization for new feedstocks and energy sources. *Comput Chem Eng*. 2018;113:209-221.
3. Zhang Q, Grossmann IE. Planning and scheduling for industrial demand side management: advances and challenges. In: Martín MM, ed. *Alternative Energy Sources and Technologies Engineering*. Springer; 2016:383-414.
4. Baldea M, Harjunkoski I. Integrated production scheduling and process control: a systematic review. *Comput Chem Eng*. 2014;71:377-390.
5. Daoutidis P, Lee JH, Harjunkoski I, Skogestad S, Baldea M, Georgakis C. Integrating operations and control: a perspective and roadmap for future research. *Comput Chem Eng*. 2018;115:179-184.
6. Seborg DE, Edgar TF, Mellichamp DA, Doyle FJ. *Process Dynamics and Control*. 3rd ed. Wiley; 2010.
7. Voll P, Klaffke C, Hennen M, Bardow A. Automated superstructure-based synthesis and optimization of distributed energy supply systems. *Energy*. 2013;50:374-388.
8. Bahl B, Lampe M, Voll P, Bardow A. Optimization-based identification and quantification of demand-side management potential for distributed energy supply systems. *Energy*. 2017;135:889-899.
9. Agha MH, Thery R, Hetreux G, Hait A, Le Lann JM. Integrated production and utility system approach for optimizing industrial unit operations. *Energy*. 2010;35(2):611-627.
10. Leenders L, Bahl B, Hennen M, Bardow A. Coordinating scheduling of production and utility system using a Stackelberg game. *Energy*. 2019;175:1283-1295.
11. Flores-Tlacuahuac A, Grossmann IE. Simultaneous scheduling and control of multiproduct continuous parallel lines. *Ind Eng Chem Res*. 2010;49(17):7909-7921.
12. Harjunkoski I, Nyström R, Horch A. Integration of scheduling and control—theory or practice? *Comput Chem Eng*. 2009;33(12):1909-1918.
13. Engell S, Harjunkoski I. Optimal operation: scheduling, advanced control and their integration. *Comput Chem Eng*. 2012;47:121-133.
14. Beal L, Petersen D, Pila G, Davis B, Warnick S, Hedengren J. Economic benefit from progressive integration of scheduling and control for continuous chemical processes. *Processes*. 2017;5(4):84.
15. Flores-Tlacuahuac A, Grossmann IE. Simultaneous cyclic scheduling and control of a multiproduct CSTR. *Ind Eng Chem Res*. 2006;45(20):6698-6712.
16. Caspari A, Offermanns C, Schäfer P, Mhamdi A, Mitsos A. A flexible air separation process: 2. Optimal operation using economic model predictive control. *AIChE J*. 2019;65:45-4393.
17. Otashu JI, Baldea M. Demand response-oriented dynamic modeling and operational optimization of membrane-based chlor-alkali plants. *Comput Chem Eng*. 2019;121:396-408.
18. Risbeck MJ, Maravelias CT, Rawlings JB, Turney RD. A mixed-integer linear programming model for real-time cost optimization of building heating, ventilation, and air conditioning equipment. *Energ Buildings*. 2017;142:220-235.
19. Mitra S, Sun L, Grossmann IE. Optimal scheduling of industrial combined heat and power plants under time-sensitive electricity prices. *Energy*. 2013;54:194-211.
20. Carrion M, Arroyo JM. A computationally efficient mixed-integer linear formulation for the thermal unit commitment problem. *IEEE Trans Power Syst*. 2006;21(3):1371-1378.
21. Sass S, Faulwasser T, Hollermann DE, et al. Model compendium, data, and optimization benchmarks for sector-coupled energy systems. *Comput Chem Eng*. 2020;135:106760.
22. Sass S, Mitsos A. Optimal operation of dynamic (energy) systems: when are quasi-steady models adequate? *Comput Chem Eng*. 2019;124:133-139.
23. Harjunkoski I, Maravelias CT, Bongers P, et al. Scope for industrial applications of production scheduling models and solution methods. *Comput Chem Eng*. 2014;62:161-193.
24. Du J, Park J, Harjunkoski I, Baldea M. A time scale-bridging approach for integrating production scheduling and process control. *Comput Chem Eng*. 2015;79:59-69.
25. Baldea M, Du J, Park J, Harjunkoski I. Integrated production scheduling and model predictive control of continuous processes. *AIChE J*. 2015;61(12):4179-4190.
26. Pattison RC, Touretzky CR, Johansson T, Harjunkoski I, Baldea M. Optimal process operations in fast-changing electricity markets: framework for scheduling with low-order dynamic models and an air separation application. *Ind Eng Chem Res*. 2016;55(16):4562-4584.
27. Kelley MT, Pattison RC, Baldick R, Baldea M. An efficient MILP framework for integrating nonlinear process dynamics and control in optimal production scheduling calculations. *Comput Chem Eng*. 2018;110:35-52.
28. Kelley MT, Pattison RC, Baldick R, Baldea M. An MILP framework for optimizing demand response operation of air separation units. *Appl Energy*. 2018;222:951-966.
29. Biegler LT. *Nonlinear Programming: Concepts, Algorithms, and Applications to Chemical Processes*. Society for Industrial and Applied Mathematics; 2010.
30. Baader FJ, Mork M, Xhonneux A, Müller D, Bardow A, Dahmen M. Mixed-integer dynamic scheduling optimization for demand side management. In: Pierucci S, Manenti F, Bozzano GL, Manca D, eds. *30th European Symposium on Computer Aided Process Engineering, Vol. 48 of Computer Aided Chemical Engineering*. Elsevier; 2020:1405-1410.
31. Corriou JP. *Process Control: Theory and Applications*. 2nd ed. Springer; 2018.
32. Daoutidis P, Kravaris C. Dynamic output feedback control of minimum-phase nonlinear processes. *Chem Eng Sci*. 1992;47(4):837-849.
33. Tsay C, Baldea M. 110th anniversary: using data to bridge the time and length scales of process systems. *Ind Eng Chem Res*. 2019;58(36):16696-16708.
34. Castro PM, Harjunkoski I, Grossmann IE. New continuous-time scheduling formulation for continuous plants under variable electricity cost. *Ind Eng Chem Res*. 2009;48(14):6701-6714.

35. Dias LS, Pattison RC, Tsay C, Baldea M, Ierapetritou MG. A simulation-based optimization framework for integrating scheduling and model predictive control, and its application to air separation units. *Comput Chem Eng*. 2018;113:139-151.
36. Remigio JEJ, Swartz CLE. Production scheduling in dynamic real-time optimization with closed-loop prediction. *J Process Control*. 2020;89:95-107.
37. Nicholson B, Siirola JD, Watson JP, Zavala VM, Biegler LT. Pyomo.dae: a modeling and automatic discretization framework for optimization with differential and algebraic equations. *Math Program Comput*. 2018;10(2):187-223.
38. Schäfer P, Daun TM, Mitsos A. Do investments in flexibility enhance sustainability? A simulative study considering the German electricity sector. *AIChE J*. 2020;66(11):e17010.
39. Petersen D, Beal L, Prestwich D, Warnick S, Hedengren J. Combined noncyclic scheduling and advanced control for continuous chemical processes. *Processes*. 2017;5(4):83.
40. Glover F. Improved linear integer programming formulations of nonlinear integer problems. *Manage Sci*. 1975;22(4):455-460.
41. Lewis JM, Lakshmivarahan S, Dhall S. Linear least squares estimation: method of normal equations. *Dynamic Data Assimilation: A Least Squares Approach*. Cambridge University Press; 2006:99-120.
42. Neisen V, Baader FJ, Abel D. Supervisory model-based control using mixed integer optimization for stationary hybrid fuel cell systems. *IFAC-PapersOnLine*. 2018;51(32):320-325.
43. Khajavirad A, Sahinidis NV. A hybrid LP/NLP paradigm for global optimization relaxations. *Math Program Comput*. 2018;10(3):383-421.
44. Skogestad S, Morari M. Understanding the dynamic behavior of distillation columns. *Ind Eng Chem Res*. 1988;27(10):1848-1862.
45. Skogestad S, Lundström P, Jacobsen EW. Selecting the best distillation control configuration. *AIChE J*. 1990;36(5):753-764.
46. Baumgärtner NJ. *Optimization of Low-Carbon Energy Systems from Industrial to National Scale*. PhD thesis. RWTH Aachen University; 2020.
47. Baumgärtner N, Delorme R, Hennen M, Bardow A. Design of low-carbon utility systems: exploiting time-dependent grid emissions for climate-friendly demand-side management. *Appl Energy*. 2019;247:755-765.
48. Fraunhofer-Institut für Solare Energiesysteme ISE. Energy-Charts. 2022. Accessed February 2, 2022. https://energy-charts.info/
49. Gurobi Optimization, LLC, Gurobi Optimizer Reference Manual. 2021. Accessed February 2, 2021. http://www.gurobi.com

SUPPORTING INFORMATION

Additional supporting information may be found in the online version of the article at the publisher's website.

How to cite this article: Baader FJ, Bardow A, Dahmen M. Simultaneous mixed-integer dynamic scheduling of processes and their energy systems. *AIChE J*. 2022;68(8):e17741. doi:10.1002/aic.17741